

A Three-Dimensional Magnetohydrodynamic Model of Planetary Nebula Jets, Knots, and Filaments

K.H. Tsui

*Instituto de Física - Universidade Federal Fluminense
Campus da Praia Vermelha, Av. General Milton Tavares de Souza s/n
Gragoatá, 24.210-346, Niterói, Rio de Janeiro, Brasil.*

tsui@if.uff.br

ABSTRACT

The morphologies of planetary nebulae are believed to be self-organized configurations. These configurations are modeled by three-dimensional temporally self-similar magnetohydrodynamic solutions with radial flow, under the gravitational field of a central star of mass M . These solutions reproduce basic features, such as jets, point-symmetric knots, and filaments, through plasma pressure, mass density, and magnetic field lines. The time evolution function of the radial velocity starts as a slow wind and terminates as a fast wind.

Subject headings:

1. Introduction

The spherical observational features of planetary nebulae can be accounted for by the celebrated interacting wind model (Dyson and de Vries 1972, Kwok et al 1978), where the early slow wind of an intermediate mass star on the asymptotic giant branch phase is caught up by the following tenuous fast wind, generating the spherical features. The elliptic and bipolar features could also be reproduced by postulating the presence of a dense equatorial cloud (Kahn and West 1985, Mellema et al 1991), which has been imaged by high resolution instruments. Nevertheless, besides these spherical, elliptic, and bipolar features, images have also revealed point-symmetric knots (Miranda and Solf 1992, Lopez et al 1993, Balick et al 1993). These point-symmetric features plus the detection of magnetic fields in central stars (Jordan et al 2005) call for a magnetohydrodynamic (MHD) approach of planetary nebulae (Pascoli 1993, Chevalier and Luo 1994, Garcia-Segura 1997, Bogovalov and Tsinganos 1999, Matt et al 2000, Gardiner and Frank 2001). Recently, Tsui (2008) has regarded the morphologies of planetary nebulae as self-organized structures, described by temporally self-similar MHD solutions in spherical coordinates with radial velocity flow for explosions. The connection between the physical process of self-organization (Hasegawa 1985, Zhu et al 1995, Yoshida and Mahajan 2002, Kondoh et al 2004) and the mathematical analysis of self-similarity, using the Lagrangian radial label, has been discussed in detail. With axisymmetry, an equatorial plasma torus and a bipolar planetary nebula can be reproduced. In essence, current hydrodynamic and magnetofluid models attribute dynamic structures to the central star, or stars, as a cause to break the spherical isotropy, to account for the nebula morphologies, as a consequence. The self-similar approach relies on the global conservation properties of MHD plasma to reach self-organized configurations regardless of the initial conditions. The spherical isotropy of explosion is broken during the course of expansion because of the magnetic field, which is non-spherical by nature.

We follow this self-similar view that considers astrophysical phenomena with ejection origins as self-organized objects, whose configurations are solved by temporally self-similar MHD solutions (Low 1982a,b, Low 1984a,b, Osherovich et al 1993, 1995, Tsui and Tavares 2005, Tsui 2006, Tsui et al 2006). This includes active galactic nucleus (AGN) jets (Tsui and Serbeto 2007), classically treated as a steady state accretion-ejection MHD transport phenomenon from the accretion disk to the polar axis (Blandford and Payne 1982), and axisymmetric planetary nebulae. Here, we develop three-dimensional MHD solutions to describe additional planetary nebula features like jets (ansae), knots, and filaments. Unlike AGN jets that are extensive objects in galactic scales and are collimated by some physical mechanism, such as plasma pressure driven collimation (Tsui and Serbeto 2007), nebula jets are much smaller objects and are not collimated. We remark that three-dimensional self-similar MHD solutions are very rare. To

our knowledge, there is only one published work which is devised specifically for interplanetary magnetic ropes (Gibson and Low 1998), which is not suitable for astrophysical phenomena.

2. Self-Similar Formulation

The basic MHD equations in Eulerian fluid description are given by

$$\frac{\partial \rho}{\partial t} + \nabla \cdot (\rho \vec{v}) = 0 , \quad (1)$$

$$\rho \left\{ \frac{\partial \vec{v}}{\partial t} + (\vec{v} \cdot \nabla) \vec{v} \right\} = \vec{J} \times \vec{B} - \nabla p - \rho \frac{GM}{r^3} \vec{r} , \quad (2)$$

$$\frac{\partial \vec{B}}{\partial t} = -\nabla \times \vec{E} = \nabla \times (\vec{v} \times \vec{B}) , \quad (3)$$

$$\nabla \times \vec{B} = \mu \vec{J} , \quad (4)$$

$$\nabla \cdot \vec{B} = 0 , \quad (5)$$

$$\frac{\partial}{\partial t} \left(\frac{p}{\rho^\gamma} \right) + (\vec{v} \cdot \nabla) \left(\frac{p}{\rho^\gamma} \right) = 0 . \quad (6)$$

Here, ρ is the mass density, \vec{v} is the bulk velocity, \vec{J} is the current density, \vec{B} is the magnetic field, p is the plasma pressure, μ is the free space permeability, γ is the polytropic index, and M is the central mass which provides the gravitational field.

We consider a radially expanding plasma and seek self-similar solutions in time where the time evolution is described by the dimensionless evolution function $y(t)$. For this purpose, it is most convenient to think of Lagrangian fluid description, and consider the position vector of a given laminar flow fluid element $\vec{r}(t)$. Under self-similarity, the radial profile is time invariant in terms of the radial label $\eta = r(t)/y(t)$, which has the dimension of r . Physically, η is the Lagrangian radial position of a fixed fluid element. With a finite plasma, the domain of η is bounded by mass conservation

$$0 < \eta_{int} < \eta < \eta_{ext} . \quad (7)$$

As for the plasma velocity, we consider self-similar structures deriving from a spherically symmetric radial velocity which can be written as

$$\vec{v} = \frac{d\vec{r}(t)}{dt} = \left\{ \eta \frac{dy}{dt}, 0, 0 \right\} = \{v, 0, 0\} . \quad (8)$$

Our self-similar parameter η , defined through the Lagrangian fluid label, explicitly represents the fluid velocity by the time evolution function $y(t)$. This evolution function will be solved self-consistently with respect to the spatial structures of the plasma. We emphasize that self-similarity, as a method, can be applied in different ways other than the one we use here. For example, Lou and his collaborators have treated an aggregating fluid under its self-gravitational field with a similarity variable $x = r(t)/at$, where a is the sound speed, for isothermal fluid, $\gamma = 1$, (Lou and Shen 2004, Bian and Lou 2005) and for a polytropic gas, $\gamma > 1$, (Lou and Wang 2006, Lou and Gao 2006) to study relevant astrophysical phenomena. Extensions to a magnetofluid have been considered by Yu and Lou (2005) and by Lou and Wang (2007). Because of the linear dependence on time, this similarity variable x refers to a reference frame moving at speed a , which is different from the radial plasma flow velocity v . Furthermore, different from our similarity variable η , x here is not the Lagrangian label of a given fluid element. For this reason, the convective derivative remains explicit in the x representation. As a result, the similarity variable of Lou amounts to finding the plasma structures in an adequate moving frame in the Eulerian x fluid description. This resembles the analytic technique of going to a moving frame to look for stationary profile solutions for nonlinear phenomena such as nonlinear Alfvén waves, solitons, etc. Because of this fundamentally different definition of self-similarity, the nature of the phenomena intended to describe is different. Our Lagrangian label self-similarity parameter is aimed to find spatial plasma configurations, and to determine the radial plasma flow velocity, consistent to the spatial configurations, through the evolution function. Since we are considering an isotropic radial plasma flow, a natural solution would be a hydrodynamic one-dimensional expanding plasma, with radially dependent mass density ρ and plasma pressure p , and with $\vec{B} = 0$ and $\vec{J} = 0$. Nevertheless, this one-dimensional hydrodynamic solution is highly unlikely because magnetic field fluctuations can be generated from current density fluctuations, even in the absence of a pre-existing magnetic field. With the magnetic fields, which are basically a two- or three-dimensional structure, coupling to the plasma will generate likewise two- or three-dimensional ρ and p .

The independent variables are now transformed from (r, θ, ϕ, t) to (η, θ, ϕ, y) . We now proceed to determine the explicit dependence of y in each one of the physical variables with this radial velocity using functional analysis. First, making use of Eq.(8), Eq.(1) renders

$$\begin{aligned} \frac{\partial \rho}{\partial t} + \frac{1}{r^2} \frac{\partial}{\partial r} (r^2 v \rho) &= \left(\frac{\partial \rho}{\partial t} + v \frac{\partial \rho}{\partial r} \right) + \rho \left(\frac{\partial v}{\partial r} + \frac{2v}{r} \right) \\ &= \frac{\partial \rho}{\partial y} \frac{dy}{dt} + \frac{3\rho}{y} \frac{dy}{dt} = \left(\frac{\partial \rho}{\partial y} + \frac{3\rho}{y} \right) \frac{dy}{dt} = 0 . \end{aligned} \quad (9a)$$

To reach the second equality, we note that the first bracket in the first equality corresponds to the total time derivative of an Eulerian fluid element which amounts to the time derivative of a Lagrangian fluid element. As for the second bracket, it can be reduced by using $v = dr/dt = \eta dy/dt$ and $\partial v/\partial r = (1/y)(dy/dt)$. Solving this equation for the y scaling by separating the time part gives

$$\rho(\vec{r}, t) = \frac{1}{y^3} \bar{\rho}(\eta, \theta, \phi) . \quad (9b)$$

As for Eq.(6), with $\alpha_0 F = (p/\rho^\gamma)$ where α_0 is a constant that carries the physical dimension so that F is a dimensionless function, it follows

$$\frac{\partial F}{\partial t} + v \frac{\partial F}{\partial r} = \frac{\partial F}{\partial y} \frac{dy}{dt} = 0 , \quad (10a)$$

$$\left(\frac{p}{\rho^\gamma} \right) = \alpha_0 F(\vec{r}, t) = \frac{1}{y^0} \alpha_0 \bar{F}(\eta, \theta, \phi) . \quad (10b)$$

As for Eq.(3), with the aid of Eq.(5), the magnetic fields are

$$\begin{aligned} \frac{\partial B_r}{\partial t} + v \frac{1}{r^2} \frac{\partial}{\partial r} (r^2 B_r) &= \left(\frac{\partial B_r}{\partial t} + v \frac{\partial B_r}{\partial r} \right) + \frac{2v}{r} B_r \\ &= \frac{\partial B_r}{\partial y} \frac{dy}{dt} + \frac{2B_r}{y} \frac{dy}{dt} = \left(\frac{\partial B_r}{\partial y} + \frac{2B_r}{y} \right) \frac{dy}{dt} = 0 , \end{aligned} \quad (11a)$$

$$B_r(\vec{r}, t) = \frac{1}{y^2} \bar{B}_r(\eta, \theta, \phi) , \quad (11b)$$

$$\begin{aligned} \frac{\partial B_\theta}{\partial t} + \frac{1}{r} \frac{\partial}{\partial r} (rv B_\theta) &= \left(\frac{\partial B_\theta}{\partial t} + v \frac{\partial B_\theta}{\partial r} \right) + \frac{1}{r} B_\theta \frac{\partial}{\partial r} (rv) \\ &= \frac{\partial B_\theta}{\partial y} \frac{dy}{dt} + \frac{2B_\theta}{y} \frac{dy}{dt} = \left(\frac{\partial B_\theta}{\partial y} + \frac{2B_\theta}{y} \right) \frac{dy}{dt} = 0 , \end{aligned} \quad (12a)$$

$$B_\theta(\vec{r}, t) = \frac{1}{y^2} \bar{B}_\theta(\eta, \theta, \phi) , \quad (12b)$$

$$\frac{\partial B_\phi}{\partial t} + \frac{1}{r} \frac{\partial}{\partial r} (rv B_\phi) = 0 , \quad (13a)$$

$$B_\phi(\vec{r}, t) = \frac{1}{y^2} \bar{B}_\phi(\eta, \theta, \phi) . \quad (13b)$$

Making use of Eq.(9b), we derive the plasma pressure from Eq.(10b)

$$p(\vec{r}, t) = \frac{1}{y^{3\gamma}} \alpha_0 \bar{F}(\eta, \theta, \phi) \bar{\rho}^\gamma(\eta, \theta, \phi) = \frac{1}{y^{3\gamma}} \alpha_0 \bar{F} \bar{\rho}^\gamma = \frac{1}{y^{3\gamma}} \bar{p}(\eta, \theta, \phi) . \quad (14)$$

Since Eq.(12a) and Eq.(13a) are of the same form, we conclude that, under self-similarity, \bar{B}_ϕ is a linear functional of \bar{B}_θ with

$$\bar{B}_\phi = k \bar{B}_\theta . \quad (15)$$

Making use of Eq.(4) to eliminate the current density in Eq.(2), we get the momentum equation which has three components. The ϕ , θ , and r components are respectively

$$\bar{B}_\theta \left[\frac{\partial}{\partial \theta} (k \bar{B}_\theta \sin \theta) - \frac{\partial \bar{B}_\theta}{\partial \phi} \right] - \bar{B}_r \left[\frac{\partial \bar{B}_r}{\partial \phi} - \sin \theta \frac{\partial}{\partial \eta} (\eta k \bar{B}_\theta) \right] - y^{4-3\gamma} \frac{\partial}{\partial \phi} (\mu \bar{p}) = 0 , \quad (16)$$

$$k \bar{B}_\theta \left[\frac{\partial}{\partial \theta} (k \bar{B}_\theta \sin \theta) - \frac{\partial \bar{B}_\theta}{\partial \phi} \right] + \bar{B}_r \left[\sin \theta \frac{\partial \bar{B}_r}{\partial \theta} - \sin \theta \frac{\partial}{\partial \eta} (\eta \bar{B}_\theta) \right] + y^{4-3\gamma} \sin \theta \frac{\partial}{\partial \theta} (\mu \bar{p}) = 0 , \quad (17)$$

$$\begin{aligned} k \bar{B}_\theta \left[\frac{1}{\eta \sin \theta} \frac{\partial \bar{B}_r}{\partial \phi} - \frac{1}{\eta} \frac{\partial}{\partial \eta} (\eta k \bar{B}_\theta) \right] - \bar{B}_\theta \left[\frac{1}{\eta} \frac{\partial}{\partial \eta} (\eta \bar{B}_\theta) - \frac{1}{\eta} \frac{\partial \bar{B}_r}{\partial \theta} \right] - y^{4-3\gamma} \frac{\partial}{\partial \eta} (\mu \bar{p}) \\ = \mu \bar{\rho} y^2 \frac{d^2 y}{dt^2} + \mu \bar{\rho} \frac{GM}{\eta^2} . \end{aligned} \quad (18)$$

We have reduced the general set of time-dependent ideal MHD equations, Eqs.(1-6), to a set of self-similar equations with appropriate time scalings, Eqs.(7-13). The general ideal MHD set has nonlinear terms of convective type $(\vec{v} \cdot \nabla)$. By using the fluid label description, the $(\vec{v} \cdot \nabla)$ convective terms are absorbed in the Lagrangian time derivative representation. The structure of the nonlinear terms, absorbed in the Lagrangian fluid label formulation, will appear in the η profile of the system.

3. Jet Structures

After this self-similar formulation, we have to solve Eqs.(16-18) for the self-similar configurations. To solve these equations, we first separate the radial variable from the other two variables by writing

$$\bar{B}_r(\eta, \theta, \phi) = A_0 R(\eta) \tilde{B}_r(\theta, \phi) , \quad (19)$$

and likewise for \bar{B}_θ , where $\bar{B}_\phi = k \bar{B}_\theta$. Furthermore, we take

$$\bar{p}(\eta, \theta, \phi) = p_0 R^2(\eta) \tilde{p}(\theta, \phi) . \quad (20)$$

Here, $R(\eta)$, $\tilde{B}_r(\theta, \phi)$, and $\tilde{p}(\theta, \phi)$ are dimensionless functions, and A_0 and p_0 carry the dimensions of magnetic field and pressure respectively. We have taken an $R^2(\eta)$ dependence because plasma pressure is a quadratic positive quantity. We take $A_0 = 1$ for unit amplitude magnetic fields, such that p_0 is relative to this amplitude. Specifically, we take

$$R(\eta) = (a\eta)^{-n} , \quad (21)$$

to represent a power law decaying field with distance, where a is a normalizing parameter of η . Considering $(4 - 3\gamma) = 0$, Eqs.(16,17) are respectively

$$\tilde{B}_\theta \left[\frac{\partial}{\partial \theta} (k \tilde{B}_\theta \sin \theta) - \frac{\partial \tilde{B}_\theta}{\partial \phi} \right] - \tilde{B}_r (n - 1) \sin \theta k \tilde{B}_\theta - \frac{\partial}{\partial \phi} \left(\frac{1}{2} \tilde{B}_r^2 + \mu p_0 \tilde{p} \right) = 0 , \quad (22)$$

$$k \tilde{B}_\theta \left[\frac{\partial}{\partial \theta} (k \tilde{B}_\theta \sin \theta) - \frac{\partial \tilde{B}_\theta}{\partial \phi} \right] + \tilde{B}_r (n - 1) \sin \theta \tilde{B}_\theta + \sin \theta \frac{\partial}{\partial \theta} \left(\frac{1}{2} \tilde{B}_r^2 + \mu p_0 \tilde{p} \right) = 0 , \quad (23)$$

We now separate the azimuthal dependence by writing

$$\tilde{B}_r(\theta, \phi) = \Theta_r(\theta) \Phi(\phi) , \quad (24a)$$

$$\tilde{B}_\theta(\theta, \phi) = \Theta(\theta) \Phi(\phi) , \quad (24b)$$

$$\tilde{p}(\theta, \phi) = \Theta_p^2(\theta) \Phi^2(\phi) , \quad (24c)$$

where $\tilde{B}_\phi = k\tilde{B}_\theta$. These functional dependences give Eq.(22) as

$$\Theta \frac{\partial}{\partial \theta} (k\Theta \sin \theta) - \Theta_r (n-1) \sin \theta k\Theta = [\Theta^2 - (\Theta_r^2 + 2\mu p_0 \Theta_p^2)] \frac{1}{\Phi} \frac{\partial \Phi}{\partial \phi} .$$

Considering the separation constant im , such that

$$\frac{\partial \Phi}{\partial \phi} = im\Phi , \quad (25a)$$

$$\Phi(\phi) = e^{+im\phi} = \cos m\phi + i \sin m\phi , \quad (25b)$$

we then have

$$\Theta \frac{\partial}{\partial \theta} (\Theta \sin \theta) - \Theta_r (n-1) \sin \theta \Theta = +\frac{i}{k} m [\Theta^2 - (\Theta_r^2 + 2\mu p_0 \Theta_p^2)] , \quad (26)$$

which identifies $k = +i$. Following the same procedures, Eq.(23) reads

$$\Theta \frac{\partial}{\partial \theta} (\Theta \sin \theta) - \Theta_r (n-1) \sin \theta \Theta = +m\Theta^2 + \frac{1}{2} \sin \theta \frac{\partial}{\partial \theta} (\Theta_r^2 + 2\mu p_0 \Theta_p^2) . \quad (27)$$

The left sides of these two equations are the same, which allows the right sides be equated to give

$$\sin \theta \frac{\partial \Theta_*^2}{\partial \theta} = -2m\Theta_*^2 , \quad (28a)$$

$$\Theta_*^2 = (\Theta_r^2 + 2\mu p_0 \Theta_p^2) . \quad (28b)$$

To solve for Θ_*^2 , we integrate Eq.(28a) to get

$$\ln \Theta_*^2 = -2m \int \frac{d\theta}{\sin \theta} = -2m \int \frac{\sin \theta d\theta}{\sin^2 \theta} = +\ln \left(\frac{1+x}{1-x} \right)^m , \quad (29)$$

where we have multiplied and divided the right side by $\sin \theta$ to implement the integration, and $x = \cos \theta$. This solution of Θ_*^2 is singular at $x = +1$ for positive m , and $x = -1$ for negative m . Such solution gives jet features on magnetic field lines and plasma density.

4. Special n=2 Case

To get Θ , instead of solving either Eq.(26) or Eq.(27), we make use of Eq.(5) to get

$$\nabla \cdot \vec{B} = \frac{1}{y^3} \left(\frac{1}{\eta} R(\eta) \right) \left\{ -(n-2) \tilde{B}_r + \frac{1}{\sin \theta} \left[\frac{\partial}{\partial \theta} (\sin \theta \tilde{B}_\theta) + \frac{\partial}{\partial \phi} (k \tilde{B}_\theta) \right] \right\} = 0 , \quad (30a)$$

$$\frac{\partial}{\partial \theta} (\sin \theta \Theta) = m\Theta + (n-2) \sin \theta \Theta_r . \quad (30b)$$

Subsituuting Eq.(30b) into Eq.(26) and Eq.(27) respectively gives

$$\sin \theta \Theta \Theta_r = m\Theta_*^2 , \quad (31a)$$

$$2\Theta \Theta_r = -\frac{\partial}{\partial \theta} \Theta_*^2 . \quad (31b)$$

It can be shown readily that these two equations are consistent to Eq.(28a). We note that Eq.(30b) couples Θ with Θ_r . To decouple these two functions, we consider the special, but probably practical, case of

$$n = 2 . \quad (32)$$

Multiplying over by $\sin \theta$ and defining $P(\theta) = \sin \theta \Theta$, Eq.(30b) can be integrated to give

$$P(x) = \left(\frac{1-x}{1+x} \right)^{m/2} , \quad (33a)$$

$$\Theta(x) = \frac{(1-x)^{(m-1)/2}}{(1+x)^{(m+1)/2}} , \quad (33b)$$

$$\Theta_r(x) = m \left(\frac{1+x}{1-x} \right)^{3m/2} , \quad (33c)$$

$$2\mu p_0 \Theta_p^2(x) = \left[\left(\frac{1+x}{1-x} \right)^m - m^2 \left(\frac{1+x}{1-x} \right)^{3m} \right] > 0 , \quad (33d)$$

where Eq.(33c) is obtained from Eq.(31a), and $\Theta_p^2(x)$ can be recovered from $\Theta_*^2(x)$ of Eq.(28b). From these solutions, we see that B_r and p are singular at $x = +1$ through $\Theta_r(x)$ and $\Theta_p^2(x)$,

whereas B_θ and B_ϕ are singular at $x = -1$ through $\Theta(x)$. We require the singularities be integrable in x , which demands the power of the singularities be less than unity. By inspection of the terms, we conclude that $m < 1/3$. Let us take

$$m = \frac{1}{4} , \quad (34)$$

to show $\Theta_*^2(x)$ in Fig.1 in a polar plot, $\Theta_r(x)$ and $\Theta(x)$ in Fig.2 and Fig.3 respectively. Figures 1 and 2 show an integrable singularity at $x = +1$, or $\theta = 0$. Furthermore, Fig.3 shows a weaker singularity at $x = +1$ than the one of Fig.2. However, Fig.3 shows another singularity at $x = -1$, while Fig.2 is regular at that location. As for $\Theta_p^2(x)$, the second term of Eq.(33d) exceeds the first term when

$$m\left(\frac{1+x}{1-x}\right)^m > 1 ,$$

or as x gets very close to unity. Writing $x = (1 - \delta)$, we get $(\delta/2)^m < m$, or $(\delta/2) < m^{1/m}$. With Eq.(34), we have $\delta = (1/2)^7$. Consequently, $\Theta_p^2(x)$ gets smaller as x approaches unity, and it vanishes at $x = (1 - \delta)$, beyond this point, it gets negative. To interpret this negative plasma pressure amplitude, $\Theta_p^2(x)$ now points backwards to the $x = -1$ direction in a polar plot, giving a jet structure as in Fig.4. This jet structure is along the radial magnetic field given by $\Theta_r(x)$.

As for the radial component, Eq.(18), with $(4 - 3\gamma) = 0$, it reads

$$\begin{aligned} \mu\bar{\rho}\eta y^2 \frac{d^2y}{dt^2} + \mu\bar{\rho}\frac{GM}{\eta^2} &= \left(\frac{1}{\eta}R^2\right)\tilde{B}_\theta\left[k\frac{1}{\sin\theta}\frac{\partial\tilde{B}_r}{\partial\phi} + \frac{\partial B_r}{\partial\theta}\right] + 2n\left(\frac{1}{\eta}R^2\right)(\mu p_0\tilde{p}) \\ &= \left(\frac{1}{\eta}R^2\right)\tilde{B}_\theta\left[-m\Theta_r + \sin\theta\frac{\partial\Theta_r}{\partial\theta}\right]\Phi + 2n\left(\frac{1}{\eta}R^2\right)\mu p_0(\Theta_p\Phi)^2 . \end{aligned} \quad (35)$$

With α as the separation constant, we have

$$\left(\frac{1}{\eta}R^2\right)\left\{\tilde{B}_\theta\left[-m\Theta_r + \sin\theta\frac{\partial\Theta_r}{\partial\theta}\right]\Phi + 2n\mu p_0(\Theta_p\Phi)^2\right\} = \mu\bar{\rho}\left(\frac{GM}{\eta^2} + \alpha\eta\right) , \quad (36a)$$

$$\frac{d^2y}{dt^2} = \frac{\alpha}{y^2} . \quad (36b)$$

We write the mass density as

$$\bar{\rho}(\eta, \theta, \phi) = \rho_0 \mathbf{R}(\eta) \tilde{\rho}(\theta, \phi) , \quad (37)$$

where ρ_0 carries the dimension of mass density, and $\mathbf{R}(\eta)$ and $\tilde{\rho}(\theta, \phi)$ are dimensionless functions. We can identify immediately from Eq.(35a) that

$$\mathbf{R}(\eta) = \frac{R^2}{(GM/\eta + \alpha\eta^2)} , \quad (38a)$$

$$\mu\rho_0\tilde{\rho} = \{\tilde{B}_\theta[-m\Theta_r + \sin\theta\frac{\partial\Theta_r}{\partial\theta}]\Phi + 2n\mu p_0(\Theta_p\Phi)^2\} = [2n\mu p_0\Theta_p^2 - 2m\Theta\Theta_r]\Phi^2 . \quad (38b)$$

From the first of these two equations, we deduce that α is positive, such that $\mathbf{R}(\eta)$ is analytic. As for the second equation, it reads

$$\mu\rho_0\tilde{\rho} = \{n[(\frac{1+x}{1-x})^m - m^2(\frac{1+x}{1-x})^{3m}] - 2m^2\frac{(1+x)^{(2m-1)/2}}{(1-x)^{(2m+1)/2}}\}\Phi^2 > 0 . \quad (39)$$

This mass density has a singularity at $x = +1$. With $m = 1/4$, we note that the numerator of the last term in Eq.(38), $(1+x)^{(2m-1)/2}$, has a negative power. This gives a singularity at $x = -1$. Since the power of this singularity is $-1/4$, it is also integrable as well. The mass density distribution is shown in Fig.5 with also a jet structure in the $x = -1$ direction, because of the radial magnetic field. If we consider $m < 0$ negative, we should point out that Figs.(1-5) would turn upside down. Consequently, the jet structures would be on both sides of the polar axis. Some examples of these jets appear in M2-9 Twin Jet Nebula, CRL 2688 Egg Nebula, NGC 3242, NGC 6826, NGC 7009. As for the time evolution function of Eq.(35b), we multiply over by dy/dt to get the first integral as

$$(\frac{dy}{dt})^2 = 2(H - \frac{\alpha}{y}) > 0 , \quad (40a)$$

where H is an integration constant. Knowing that α is positive, and $y(0) = 1$ by definition of Lagrangian fluid label, and the right side of this equation has to be positive, we conclude that $H > \alpha > 0$. This gives the plasma wind velocity a slow start initially with $(dy/dt)^2 = 2(H - \alpha)$ which evolves into a fast terminal wind of

$$(\frac{dy}{dt})^2 = 2H . \quad (40b)$$

5. Knot and Filament Structures

With the momentum equation solved, the magnetic fields are given by

$$\bar{B}_r = +R(\eta)\Theta_r \cos m\phi , \quad (41a)$$

$$\bar{B}_\theta = +R(\eta)\Theta \cos m\phi , \quad (41b)$$

$$\bar{B}_\phi = -R(\eta)\Theta \sin m\phi . \quad (41c)$$

The magnetic field lines are given by

$$\frac{\Theta_r \cos m\phi}{d\eta} = \frac{\Theta \cos m\phi}{\eta d\theta} = -\frac{\Theta \sin m\phi}{\eta \sin \theta d\phi} , \quad (42a)$$

which can be written as

$$\frac{d\eta}{\eta} = -m \frac{(1+x)^{2m}}{(1-x)^{2m}} dx = -m \frac{(1+x)^{2m+1}}{(1-x)^{2m-1}} \frac{d\phi}{\tan m\phi} . \quad (42b)$$

With η_0 as an integration constant, the first equality gives

$$\ln \frac{\eta}{\eta_0} = -m \int \frac{(1+x)^{2m}}{(1-x)^{2m}} dx , \quad (43a)$$

which can be integrated numerically, as is shown in Fig.6. Since the singularity is integrable, η is finite at $x = +1$. The second equality corresponds to

$$\frac{d\theta}{\sin \theta} = -\frac{d\phi}{\tan m\phi} ,$$

and can be integrated to give

$$\frac{(1+x)^m}{(1-x)^m} = K(\sin m\phi)^2 , \quad (43b)$$

where K is an integration constant. With the interval of x between $(-1, +1)$, or θ between $(\pi, 0)$, the left side of Eq.(43b), $(1+x)^m/(1-x)^m$ labelled on the left axis, covers an interval $(0, \infty)$ with positive m , and is plotted in Fig.7 against x between $(-1, +1)$ labelled on the

bottom axis. The right side, $K(\sin m\phi)^2$ labelled on the right axis, is also plotted against $m\phi$ on the top axis, with a scale between 0 and $\pi/2$, in the same figure. In order to view the mapping between the right side and the left side, we assign a large constant K . With $m = 1/4$ and $K = 3$, as x departs from -1 , or θ from π , $m\phi$ departs from 0, and it maps a root of ϕ . As x approaches $+1$, or θ approaches 0, $m\phi$ reaches $\pi/2$, which takes ϕ over $(0, 2\pi)$. On the return path of the field lines, x decreases from $+1$ back to -1 , bringing $m\phi$ from $\pi/2$ to π along the descending branch of $K(\sin m\phi)^2$, which takes ϕ over $2\pi, 4\pi$. This descending branch, which is the continuation of Fig.7, is not shown. To summarize, the field lines starting at $x = -1$ and $\eta = +1$ go through the $x = (-1, +1, -1)$ cycle once, with $\eta = (+1, +2.3, +1)$, while completing the $m\phi = (0, \pi)$ cycle once, covering $\phi = (0, 4\pi)$, before closing on themselves again. This generates helical field lines, as shown in Fig.8, on the surface of revolution of Fig.6. Since the singularities at $x = \pm 1$ are integrable, and also because of the circulating nature of the fields \bar{B}_θ and \bar{B}_ϕ , the magnetic field lines converge to $\eta = 1$ at $x = -1$ axis and to $\eta = 2.3$ at $x = +1$ axis, as shown in Fig.6. These locations correspond to point-symmetric magnetic knots, where the field strength is infinite. As for the filaments, they correspond to the helical magnetic field lines in space, as shown in Fig.8. These same field lines give a different shape when they are viewed at different orientations, such as in Fig.9 and Fig.10. Further field lines can be generated with, for example, $m = 1/3.5 = 2/7 = 4/14$. In this case, the field lines starting at $x = -1$ and $\eta = +1$ go through the $x = (-1, +1, -1)$ cycle once, with $\eta = (+1, +2.3, +1)$, while completing the $m\phi = (0, \pi/2, \pi)$ cycle once, covering $\phi = (0, 7\pi/4, 7\pi/2)$. Since the lowest 2π multiple of the ϕ cycle is four, the field lines have to complete four cycles of x and of $m\phi$ to make ϕ covering $(0, 7\pi, 14\pi)$, such that the field lines can close on themselves again. With different values of η_0 of Eq.(43a), we can fill up the space with shells of field lines of some m less than $1/3$ up to η_{ext} of Eq.(7), and dot the polar axis with a line of magnetic knots. Despite the radial component at $x = +1$ giving the plasma jet structures, the field lines are closed at $\eta = 2.3$ because of the circulating nature of the meridian and azimuthal components. With $m < 0$ negative, the mirror images of the knots and field lines can be superimposed on those with $m > 0$ positive, generating lines of knots and concentric shells of magnetic field lines. Examples of knots can be found in M2-9 Twin Jet Nebula, NGC 5307, and filaments in MyCn 18 Hourglass Nebula, NGC 6543 Cat's Eye Nebula, NGC 2392 Eskimo Nebula, M2-9 Twin Jet Nebula, NGC 6543.

6. General n Case

We now solve Eq.(30b) for an arbitrary n . Combining Eq.(30b) an Eq.(31a), we get

$$(1-x^2)\frac{d}{dx}P^2(x) + 2mP^2(x) = -2m(n-2)(1-x^2)\Theta_*^2(x) , \quad (44a)$$

where $P(x) = (1-x^2)^{1/2}\Theta(x)$ and $\Theta_*^2(x)$ is given by Eq.(29). If the boundary condition is known, this equation can be integrated numerically to get

$$P^2(x) = -2m \int_{-1}^x \left[\frac{P^2(x)}{(1-x^2)} + (n-2)\Theta_*^2(x) \right] dx + P^2(-1) . \quad (44b)$$

To obtain the boundary condition at $x = -1$, we note that the right side of Eq.(44a) is equal to $-2m(n-2)(1+x)^{m+1}/(1-x)^{m-1}$. Since $m < 1$ positive, this term vanishes at $x = -1$ and at $x = +1$ as well. As a result, in the neighborhood of $x = \pm 1$, $P^2(x)$ is described by the homogeneous version of Eq.(44a), where the right side is null. The homogeneous solution can be solved readily as

$$P^2(x) = \left(\frac{1-x}{1+x} \right)^m , \quad (45)$$

which provides the needed boundary condition. The self-similar functions are, therefore, given by

$$\Theta(x) = \frac{P(x)}{\sin \theta} , \quad (46a)$$

$$\Theta_r(x) = \frac{m\Theta_*^2(x)}{P(x)} , \quad (46b)$$

$$2\mu p_0 \Theta_p^2(x) = [\Theta_*^2(x) - \Theta_r^2(x)] > 0 , \quad (46c)$$

As for the magnetic field lines, they are described by

$$\ln \frac{\eta}{\eta_0} = -m \int \frac{\Theta_*^2(x)}{P^2(x)} dx , \quad (47a)$$

$$\frac{d\theta}{\sin \theta} = -\frac{d\phi}{\tan m\phi} . \quad (47b)$$

The second equation remains the same, while the first equation can be integrated numerically to get the field lines. With $n = 3$, the corresponding self-similar functions of Figs.2-6 are evaluated anew, and are presented in Figs.11-15 respectively. From Fig.12 and Fig.15, we can see that the source term in Eq.(44a) makes $\Theta(x)$ and the $(\eta - x)$ mapping more symmetric. The corresponding magnetic field lines are also shown in Figs.16-18, with knots, $x = \pm 1$ and $\eta = +1$, at equal distance from the center.

To conclude, we have regarded the morphologies of planetary nebulae as self-organized configurations. These configurations are modeled by temporally self-similar MHD solutions. To complement an earlier publication (Tsui 2008) for axisymmetric features, we have presented a three-dimensional self-similar model with $\gamma = 4/3$, which reproduces features like jets, point-symmetric knots, and filaments, through plasma pressure, mass density, and magnetic field lines. The time evolution function of the self-similar solutions starts the plasma expansions as a slow wind, and terminates as a fast wind. With this three-dimensional model, which completes the earlier two-dimensional axisymmetric model, we have covered most of the existing features in planetary nebulae with this self-similar approach for self-organized configurations. Considering that the extragalactic AGN polar jets could be accounted for on the same ejection basis (Tsui and Serbeto 2007), through a plasma pressure driven collimation process, which differs from the classical accretion-ejection spatially self-similar steady state MHD transport model (Blandford and Payne 1982), we believe temporally self-similar MHD configurations are universal manifestations of self-organized astrophysical ejection phenomena.

Acknowledgments

The author is deeply grateful to Dr. B.C. Low for the inspiring thoughts and physical insights of self-similar solutions, and to Prof. Akira Hasegawa for the very essential concept of self-organization in fluids and plasmas.

REFERENCES

Balick, B., Rutgers, M., Terzian, Y., and Ghengalur, J.N., 1993. Fast, Low-Ionization Emission Regions and Other Microstructures in Planetary Nebulae, *Astrophys. J.* **411**, 778-793.

Bian, F.Y. and Lou, Y.Q., 2005. Spherical Isothermal Self-Similar Shock Flows, *Mon. Not. R. Astron. Soc.* **363**, 1315-1328.

Blandford, R.D. and Payne, D.G., 1982. Hydromagnetic Flows from Accretion Discs and the Production of Radio Jets, *Mon. Not. Royal Astron. Soc.* **199**, 883-903.

Bogovalov, S. and Tsinganos, K., 1999. On the Magnetic Acceleration and Collimation of Astrophysical Outflows, *Mon. Not. Royal Astron. Soc.* **305**, 211-224.

Chevalier, R.A. and Luo, D., 1994. Magnetic Shaping of Planetary Nebulae and Other Stellar Wind Bubbles, *Astrophys. J.* **421**, 225-235.

Dyson, J.E. and de Vries, J., 1972. The Dynamical Effects of Stellar Mass Loss on Diffuse Nebulae, *Astron. and Astrophys.* **20**, 223-232.

Gardiner, T.A. and Frank, A., 2001. Magnetic Collimation in Planetary Nebulae, *Astrophys. J.* **557**, 250-255.

Garcia-Segura, G., 1997. Three-Dimensional Magnetohydrodynamic Modeling of Planetary Nebulae: The Formation of Jets, Ansae, and Point-Symmetric Nebulae via Magnetic Collimation, *Astrophys. J.* **489**, L189-L192.

Gibson, S.E. and Low, B.C. 1998. A Time-Dependent Three-Dimensional Magnetohydrodynamic Model of the Coronal Mass Ejection, *Astrophys. J.* **493**, 460-473.

Hasegawa, A., 1985. Self-Organization Processes in Continuous Media, *Adv. Phys.* **34**, 1-42.

Jordan, S., Werner, K., and OToole, S.J., 2005. Discovery of Magnetic Fields in Central Stars of Planetary Nebulae, *Astron. and Astrophys.* **432**, 273-279.

Kondoh, Y., Serizawa, S., Nakano, A., Takahashi, T., and Van Dam, J.W., 2004. Self-Organization Phenomena and Decaying Self-Similar State in Two-Dimensional Incompressible Viscous Fluids, *Phys. Rev. E* **70**, 066312.

Kahn, F.D. and West, K.A., 1985. Shapes of Planetary Nebulae, *Mon. Not. R. Astron. Soc.* **212**, 837-850.

Kwok, S., Purton, C.R., and FitzGerald, P.M., 1978. On the Origin of Planetary Nebulae, *Astrophys. J.* **219**, L125-L127.

Lopez, J.A., Meaburn, J., and Palmer, J.W. 1993. Kinematical Evidence for a Rotating, Episodic Jet in the Planetary Nebula Fleming 1, *Astrophys. J.* **415**, L135-L137.

Lou, Y.Q. and Shen, Y., 2004. Envelope Expansion with Core Collapse - I. Spherical Isothermal Similarity Solutions, *Mon. Not. R. Astron. Soc.* **348**, 717-737.

Lou, Y.Q. and Gao, Y., 2006. Self-Similar Shocks in Polytropic Gas Flows Around Star-Forming Regions, *Mon. Not. R. Astron. Soc.* **373**, 1610-1618.

Lou, Y.Q. and Wang, W.G., 2006. New Self-Similar Solutions of Polytropic Gas Dynamics, *Mon. Not. R. Astron. Soc.* **372**, 885-900.

Lou, Y.Q. and Wang, W.G., 2007. Magnetohydrodynamic Rebound Shocks of Supernovae, arXiv 0704.0223v1 [astro-ph].

Low, B.C., 1982a. Self-Similar Magnetohydrodynamics. I. The $\gamma = 4/3$ Polytrope and the Coronal Transient, *Astrophys. J.* **254**, 796-805.

Low, B.C., 1982b. Self-Similar Magnetohydrodynamics. II. The Expansion of a Stellar Envelope into a Surrounding Vacuum, *Astrophys. J.* **261**, 351-369.

Low, B.C., 1984a. Self-Similar Magnetohydrodynamics. III. The Subset of Spherically Symmetric Gasdynamic Flows, *Astrophys. J.* **281**, 381-391.

Low, B.C., 1984b. Self-Similar Magnetohydrodynamics. IV. The Physics of Coronal Transients, *Astrophys. J.* **281**, 392-412.

Matt, S., Balick, B., Winglee, R., and Goodson, A., 2000. Disk Formation by Asymptotic Giant Branch Winds in Dipole Magnetic Fields, *Astrophys. J.* **545**, 965-973.

Mellema, G., Eulderink F., and Icke, V., 1991. Hydrodynamical Models of Aspherical Planetary Nebulae, *Astron. and Astrophys.* **252**, 718-732.

Miranda, L.F., and Solf, J., 1992. Long-Slit Spectroscopy of the Planetary Nebula NGC6543: Collimated Bipolar Ejections From a Precessing Central source?, *Astron. and Astrophys.* **260**, 397-410.

Osherovich, V.A., Farrugia, C.J., and Burlaga, L.F., 1993. Nonlinear Evolution of Magnetic Flux Ropes. 1. Low-Beta Limit, *J. Geophys. Res.* **98**, 13225-13231.

Osherovich, V.A., Farrugia, C.J., and Burlaga, L.F., 1995. Nonlinear Evolution of Magnetic Flux Ropes. 2. Finite-Beta Plasma, *J. Geophys. Res.* **100**, 12307-12318.

Pascoli, G., 1993. Bipolar Jets in Planetary Nebulae: An Analytical Model, *J. Astrophys. Astr.* **14**, 65-82.

Tsui, K.H., 2006. A Self-Similar Magnetohydrodynamic Model for Ball Lightnings, *Phys. Plasmas* **13**, 072102.

Tsui, K.H., 2008. Magnetohydrodynamic Model of Equatorial Plasma Torus in Planetary Nebulae, *Astron. Astrophys.* , to be published.

Tsui, K.H., Navia, C.E., Robba, M.B., Carneiro, L.T., and Emelin, S.E., 2006. Self-Similar Magnetohydrodynamic Model for Direct Current Discharge Fireball Experiments, *Phys. Plasmas* **13**, 113503.

Tsui, K.H. and Serbeto, A., 2007. Time-Dependent Magnetohydrodynamic Self-Similar Extra-galactic Jets, *Astrophys. J.* **658**, 794-803.

Tsui, K.H. and Tavares, M.D., 2005. Self-Similar Evolution of the Two-Dimensional Cylindrical Magnetohydrodynamic Flux Rope, *J. Atmos. Solar-Terr. Phys.* **67**, 1691-1696.

Yoshida, Z. and Mahajan, S.M., 2002. Variational Principles and Self-Organization in Two-Fluid Plasmas, *Phys. Rev. Lett.* **88**, 095001.

Yu, C. and Lou, Y.Q., 2005. Envelope Expansion with Core Collapse - II. Quasi-Spherical Self-Similar Solutions for an Isothermal Magnetofluid, *Mon. Not. R. Astron. Soc.* **364**, 1168-1184.

Zhu, S.P., Horiuchi, R., Sato, T., and Complexity Simulation Group, 1995. Non-Taylor Magnetohydrodynamic Self-Organization, *Phys. Rev. E* **51**, 6047-6054.

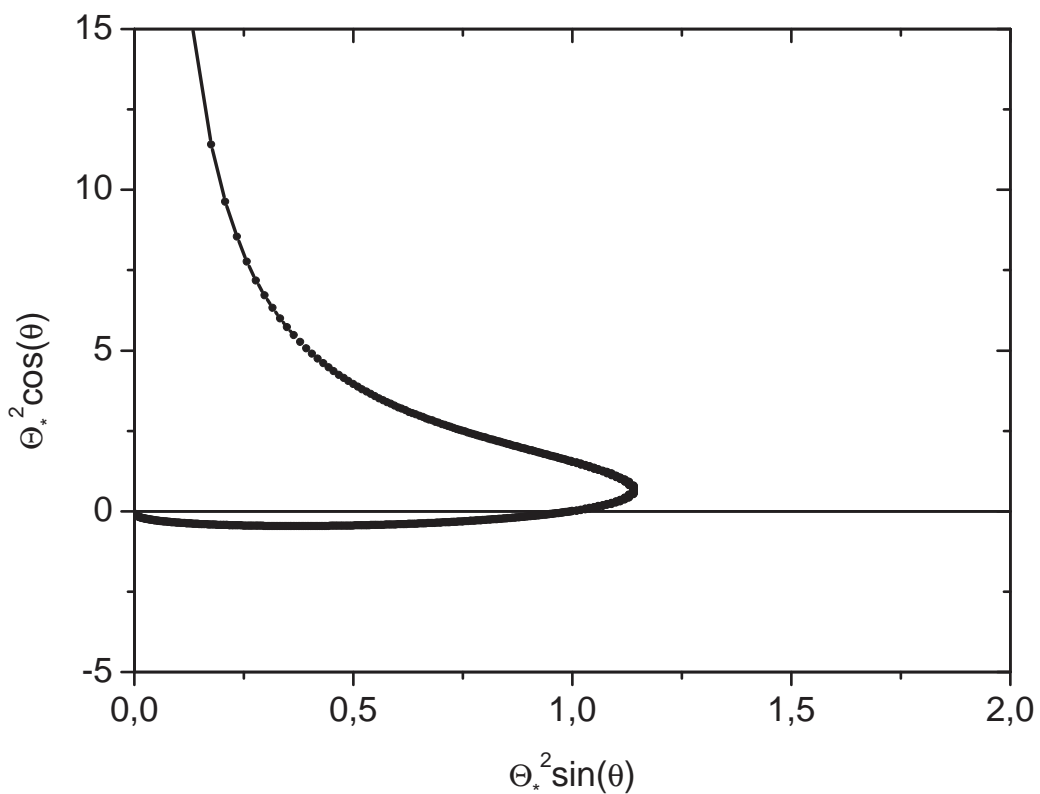


Fig. 1.— The function $\Theta_*^2(x)$ with $x = \cos \theta$ is shown in a polar plotted indicating an integrable singularity at $x = +1$ for a jet structure.

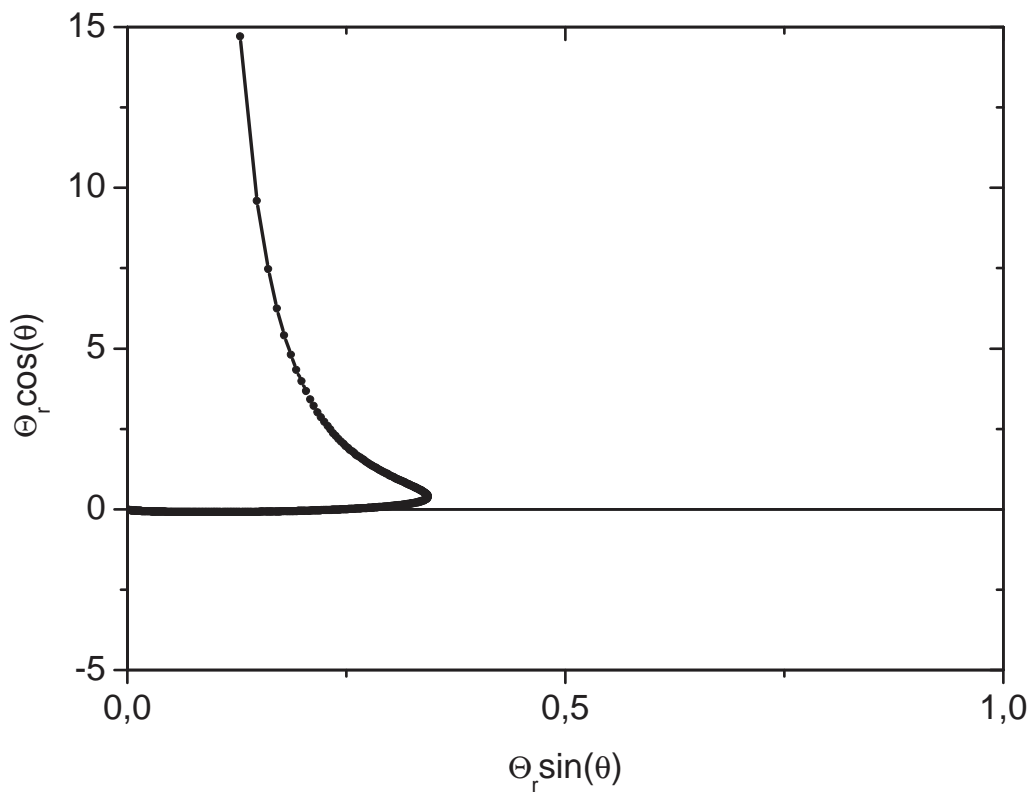


Fig. 2.— The function $\Theta_r(x)$ with $x = \cos \theta$ is shown in a polar plotted indicating an integrable singularity at $x = +1$ for a jet structure.

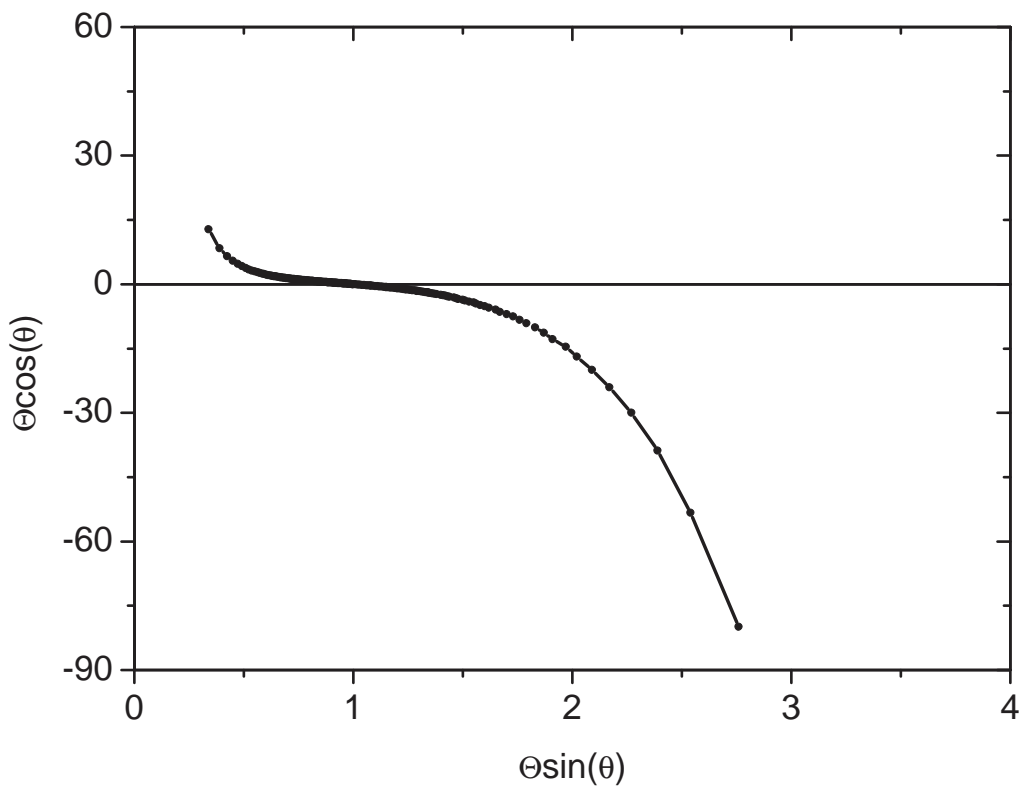


Fig. 3.— The function $\Theta(x)$ with $x = \cos \theta$ is shown in a polar plotted indicating integrable singularities at $x = +1$ and at $x = -1$ for knot structures.

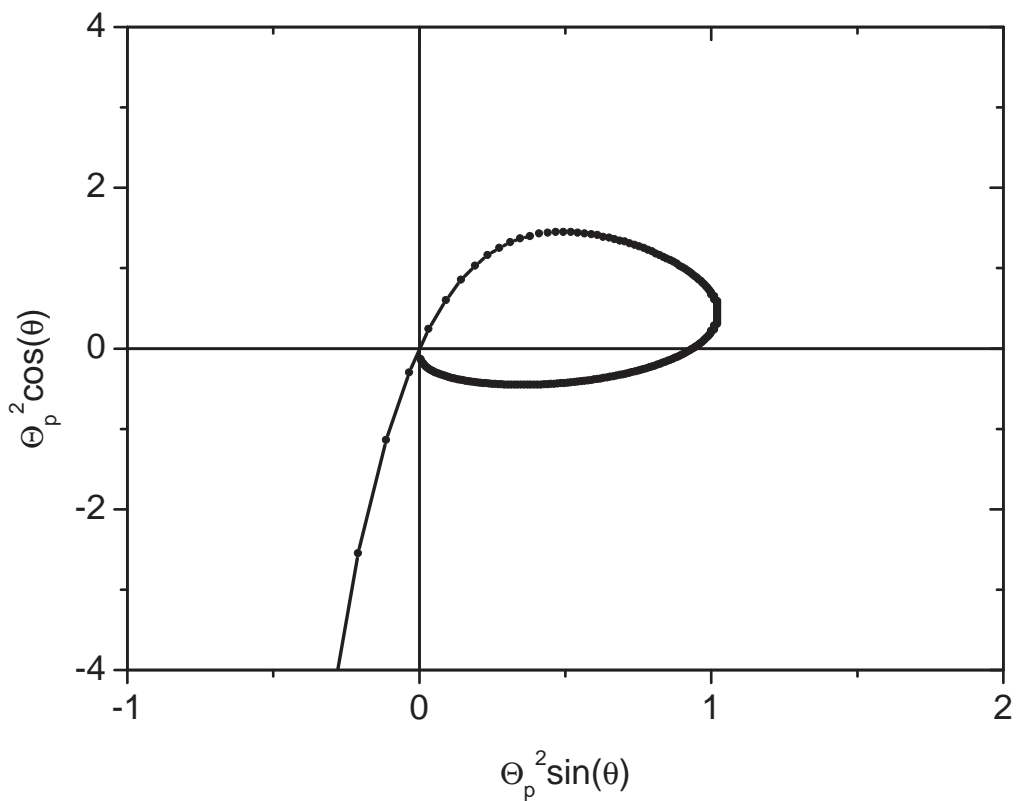


Fig. 4.— The function $\Theta_p^2(x)$ with $x = \cos \theta$ is shown in a polar plotted indicating a plasma pressure jet in a very narrow cone about $x = +1$.

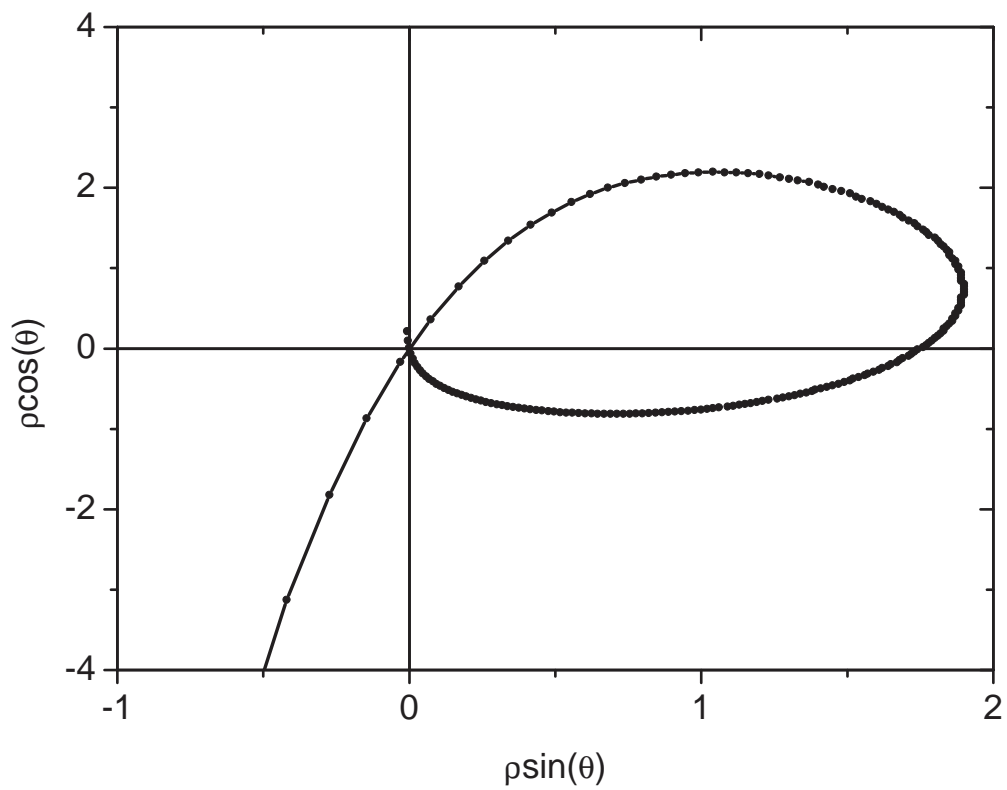


Fig. 5.— The function $\tilde{\rho}(x)$ with $x = \cos \theta$ is shown in a polar plotted indicating a mass density jet in a very narrow cone about $x = +1$.

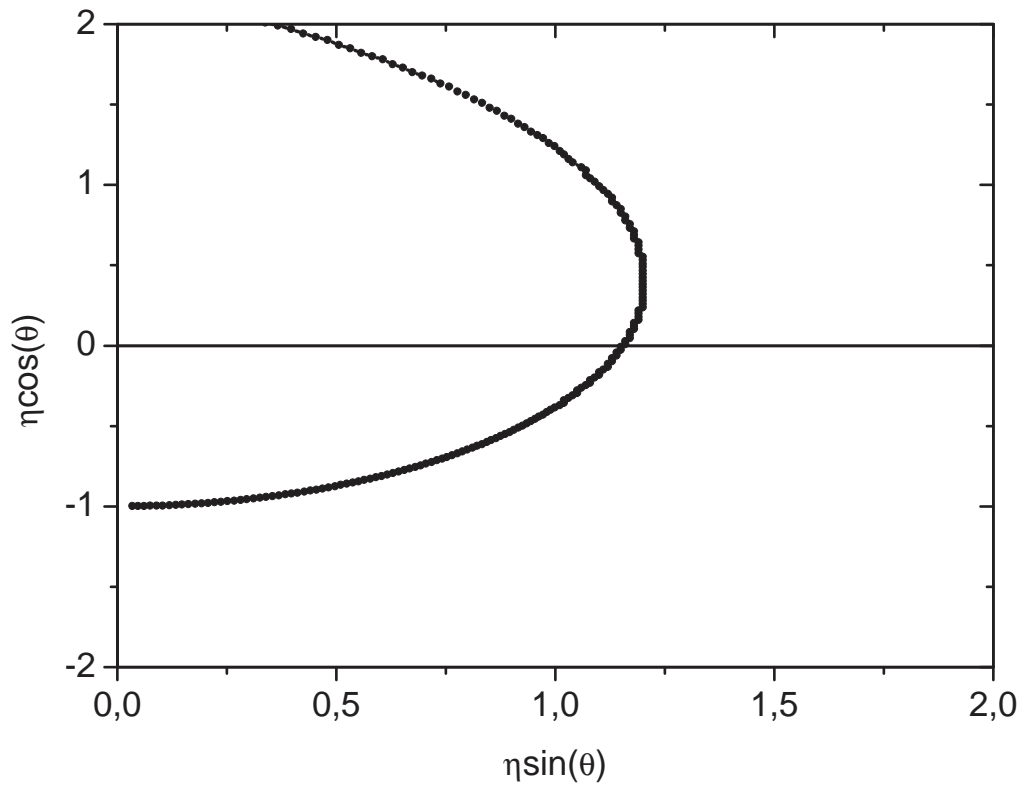


Fig. 6.— The magnetic field line $\eta - \theta$ dependence is shown in a polar plotted.

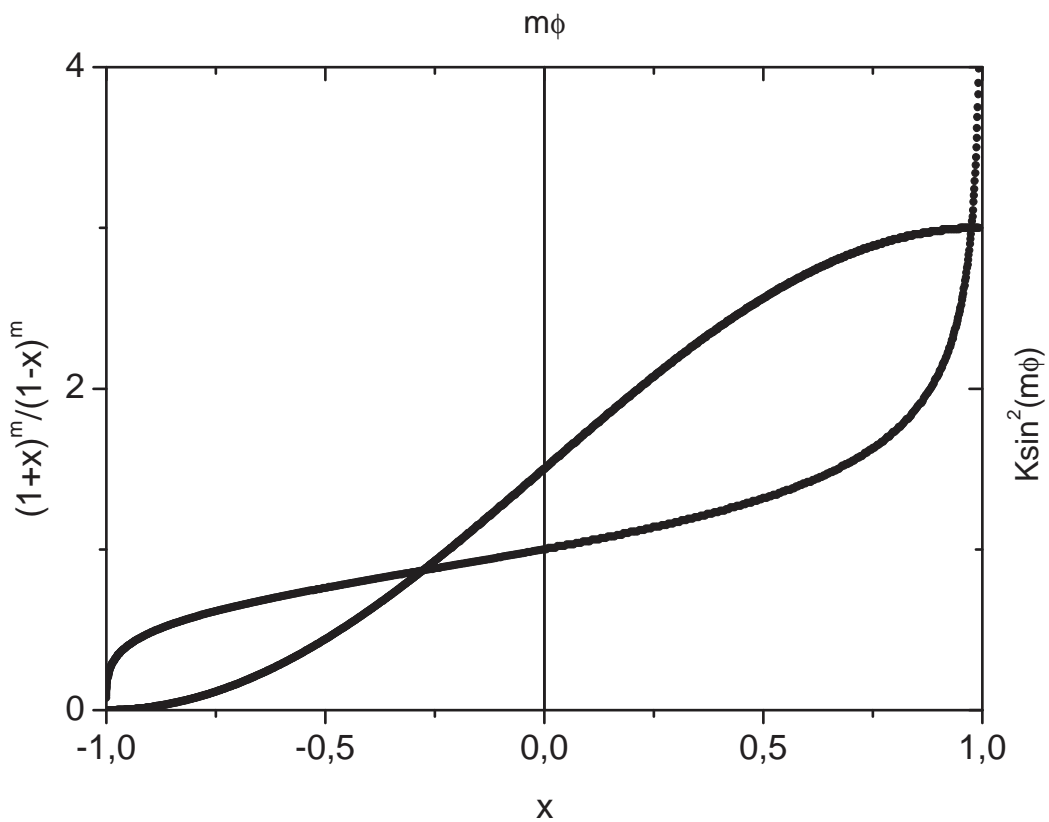


Fig. 7.— The magnetic field line $\phi - \theta$ dependence is shown in a parametric plotted.

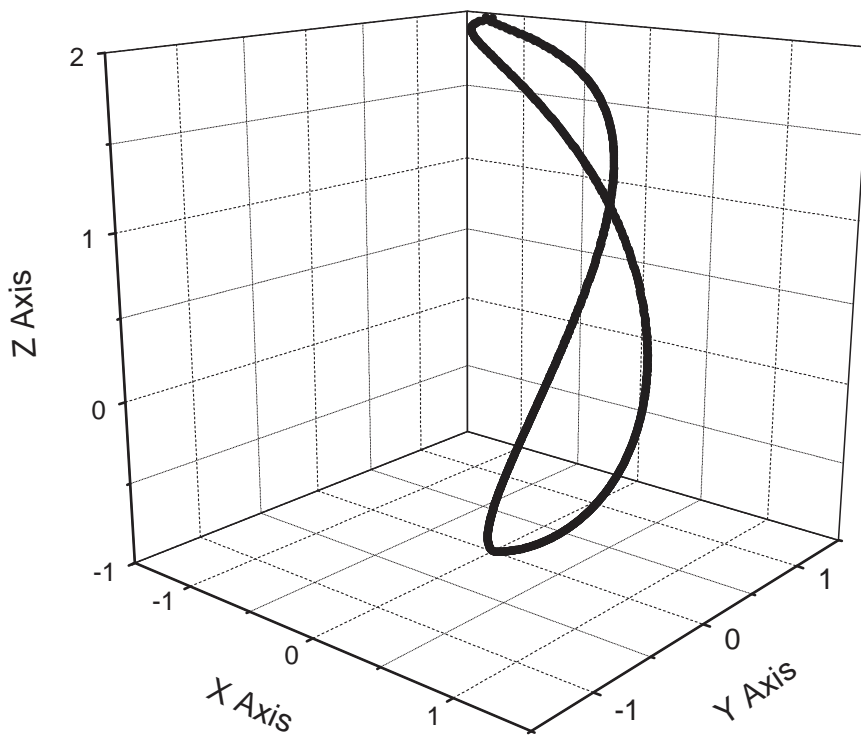


Fig. 8.— The three-dimensional magnetic field lines, wound on the surface of revolution of Fig.6, are viewed parallel to the x-y plane at about 45 degrees.

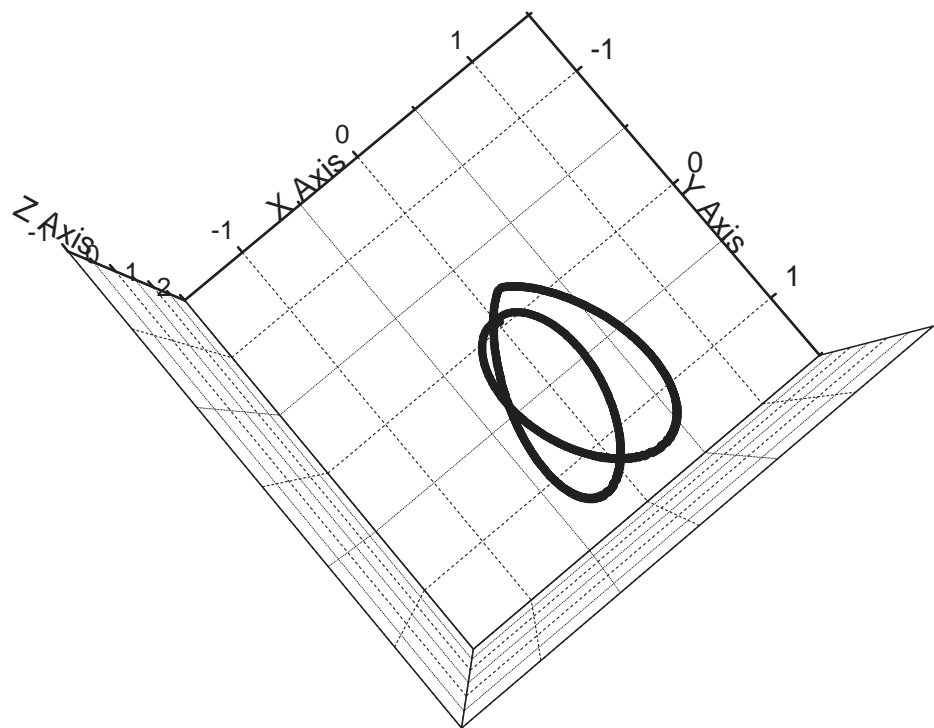


Fig. 9.— The three-dimensional magnetic field lines, wounded on the surface of revolution of Fig.6, are viewed down the z axis.

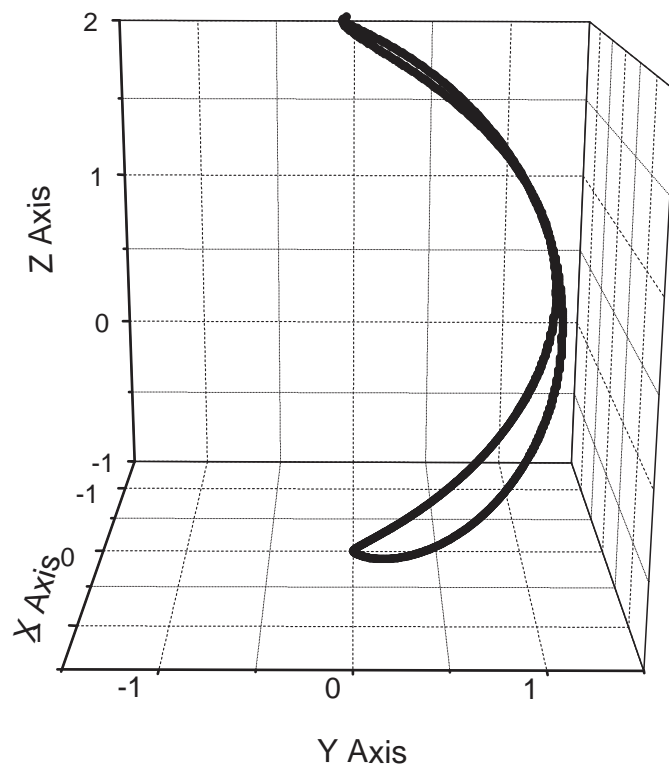


Fig. 10.— The three-dimensional magnetic field lines, wounded on the surface of revolution of Fig.6, are viewed along the x axis.

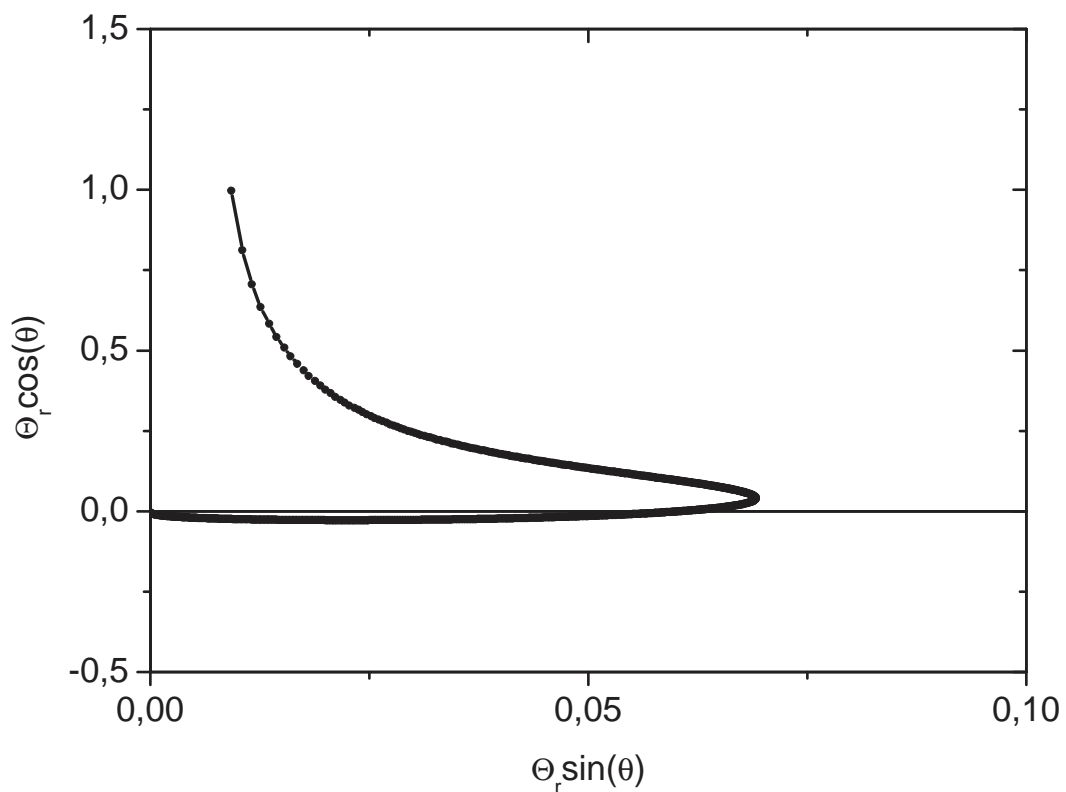


Fig. 11.— The function $\Theta_r(x)$, with $n = 3$, is shown in a polar plotted indicating an integrable singularity at $x = +1$ for a jet structure.

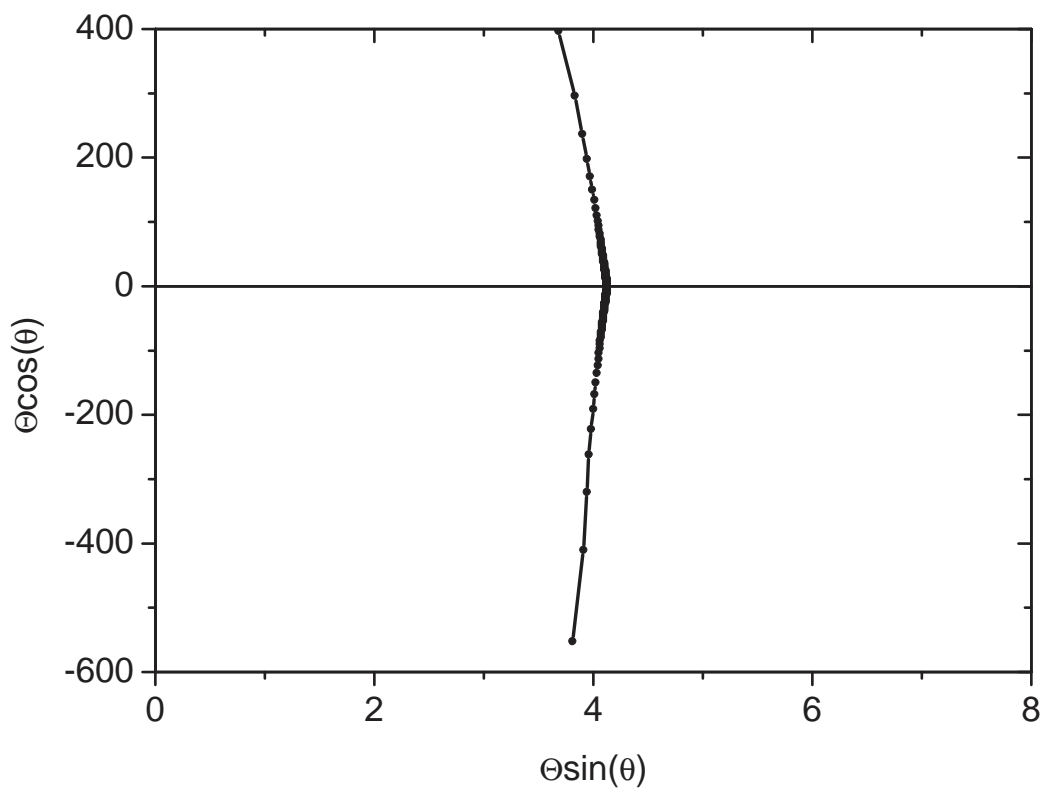


Fig. 12.— The function $\Theta(x)$, with $n = 3$, is shown in a polar plotted indicating a more symmetric structure.

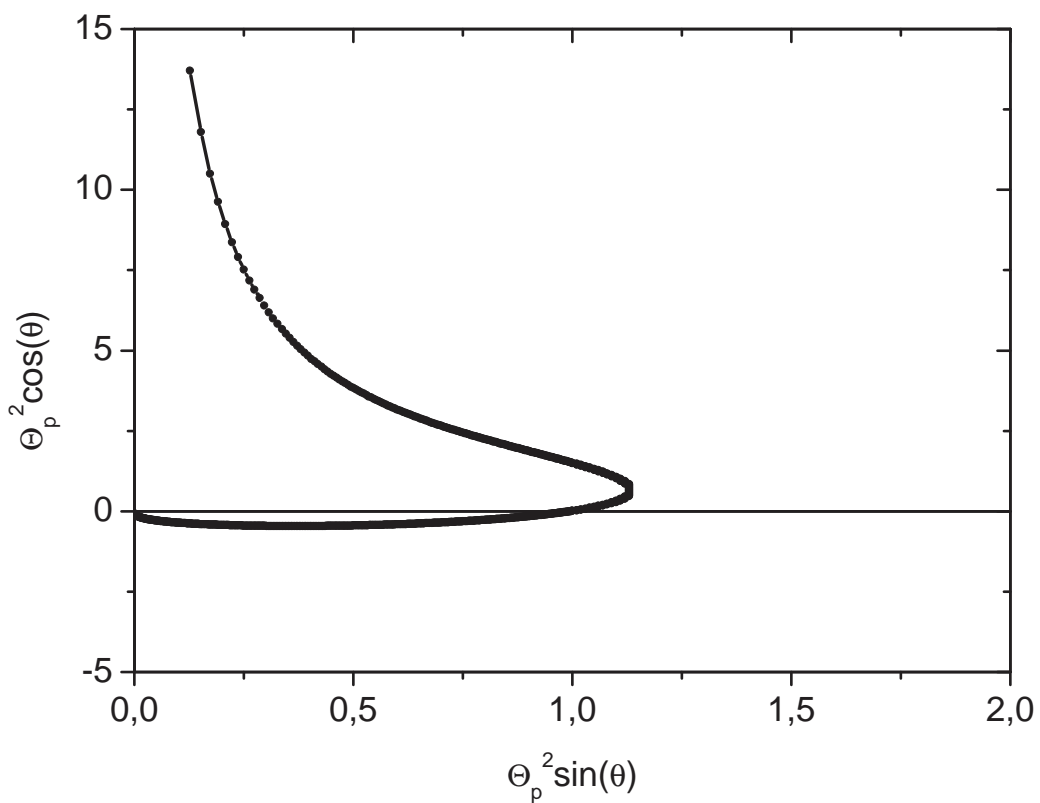


Fig. 13.— The function $\Theta_p^2(x)$, with $n = 3$, is shown in a polar plotted indicating a plasma pressure jet in a very narrow cone about $x = +1$.

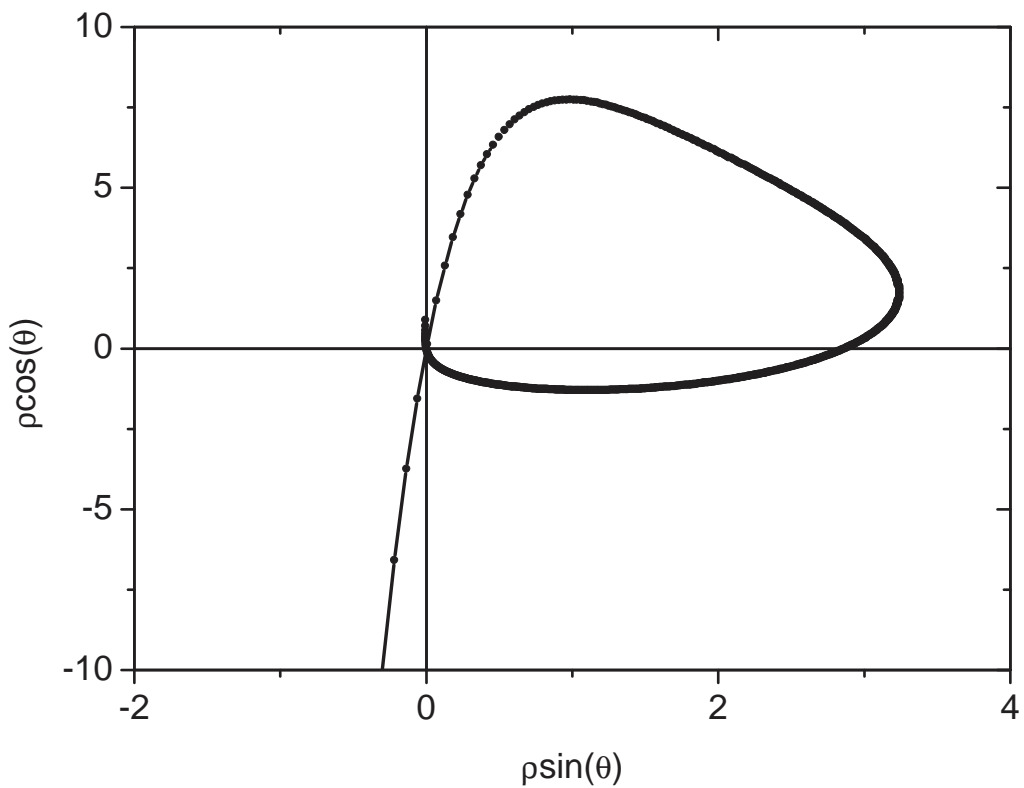


Fig. 14.— The function $\tilde{\rho}(x)$ with $n = 3$ is shown in a polar plotted indicating a mass density jet in a very narrow cone about $x = +1$.

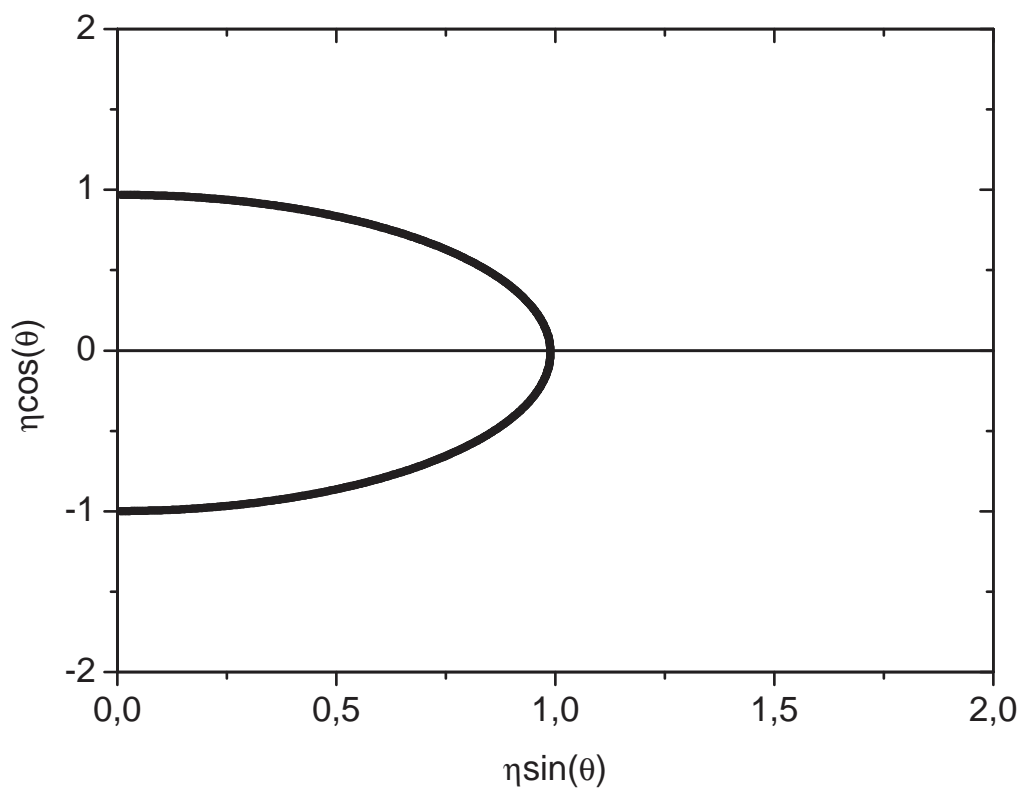


Fig. 15.— The magnetic field line $\eta - \theta$ dependence, with $n = 3$, is shown in a polar plotted showing a symmetric structure.

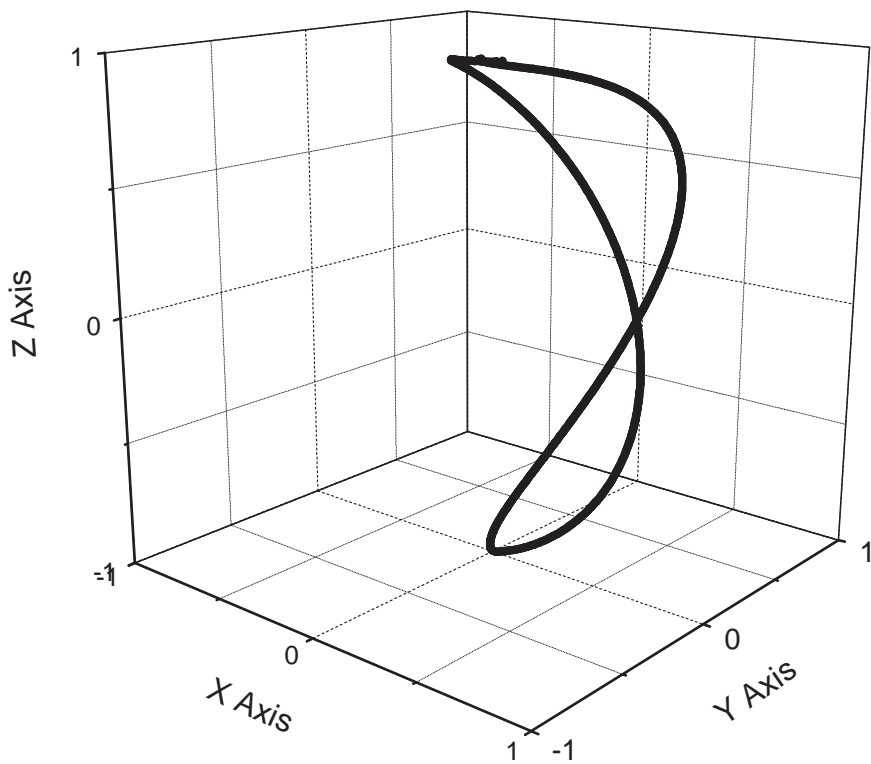


Fig. 16.— The three-dimensional magnetic field lines, with $n = 3$, are viewed parallel to the x-y plane at about 45 degrees.

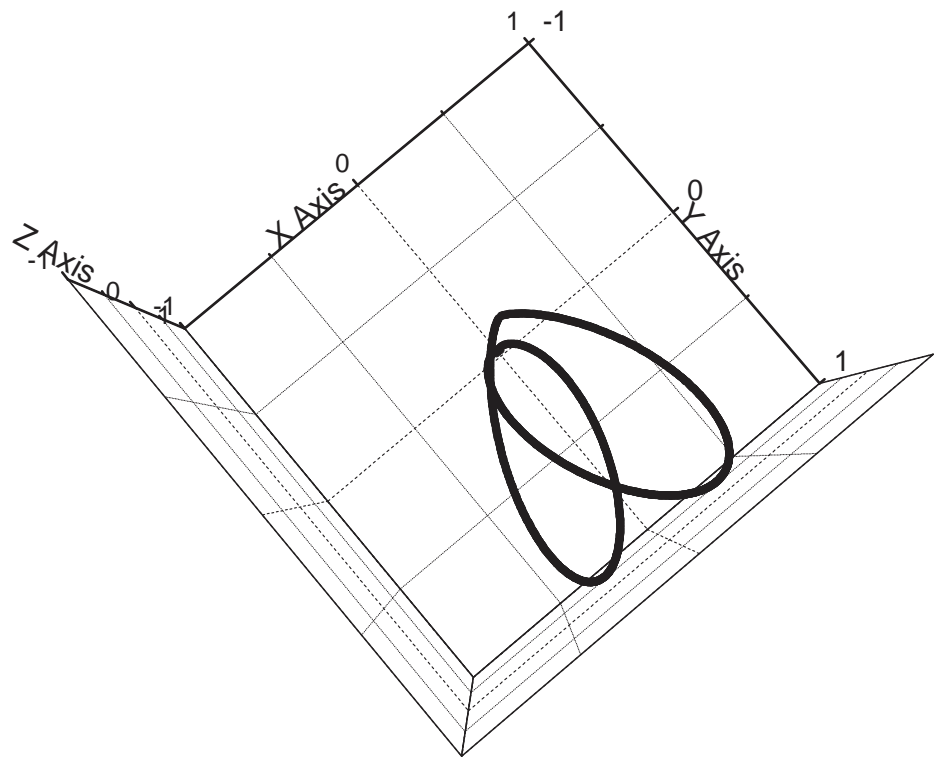


Fig. 17.— The three-dimensional magnetic field lines, with $n = 3$, are viewed down the z axis.

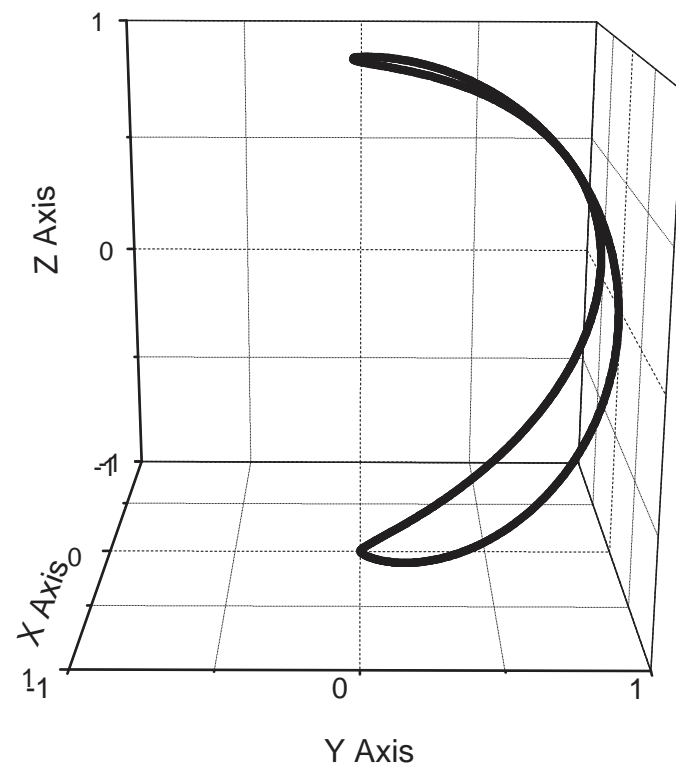


Fig. 18.— The three-dimensional magnetic field lines, with $n = 3$, are viewed along the x axis.